Size and solvation effects on electronic and optical properties of PbS quantum dots

Benoît Sklénard, Gabriel Mugny, Bilal Chehaibou, Christophe Delerue, Arthur Arnaud, Jing Li

Size and Solvation Effects on Electronic and Optical Properties of PbS Quantum Dots

Benoît Sklénard,[†] Gabriel Mugny,[‡] Bilal Chehaibou,[¶] Christophe Delerue,[¶] Arthur Arnaud,[§] and Jing Li[*,†]

[†]*Univ. Grenoble Alpes, CEA, Leti, F-38000, Grenoble, France*

[‡]*STMicroelectronics, 12 rue Jules Horowitz, 38019 Grenoble, France*

[¶]*Univ. Lille, CNRS, Centrale Lille, Univ. Polytechnique Hauts-de-France, Junia, UMR 8520—IEMN, F-59000 Lille, France*

[§]*STMicroelectronics, 850 rue J. Monnet, 38926 Crolles, France*

E-mail: Jing.Li@cea.fr

Abstract

PbS quantum dots (QDs), among the most mature nanocrystals obtained by colloidal chemistry, are promising candidates in optoelectronic applications at various operational frequencies. QD device performances are often determined by charge transport, either carrier injection before photoemission or charge detection after photoabsorption, which is significantly influenced by the dielectric environment. Here, we present the electronic structure and the optical gap of PbS QDs versus size for various solvents calculated using *ab initio* methods including the many-body perturbation approaches. This study highlights the importance of the dielectric environment, pointing out 1) the non-negligible shift of the electronic structure due to the ground state polarization; 2) a substantial impact on the electronic bandgap. The electron-hole binding energy, which varies largely with the QD size and solvent, is well-described by

an electrostatic model. This study reveals the fundamental physics of size and solvation effects, which could be useful to design PbS QDs-based optoelectronic devices.

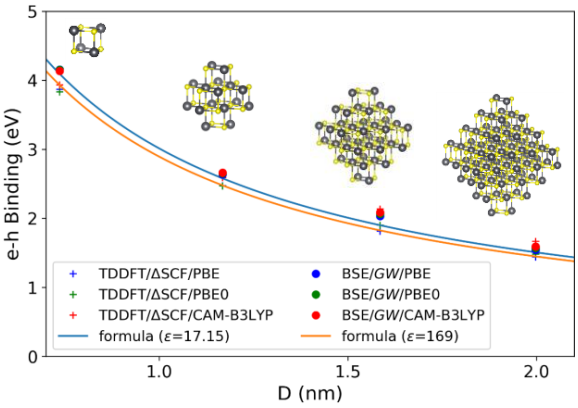

Introduction PbS quantum dots (QDs) are promising candidates in various optoelectronic applications, such as lasers,[1,2] light-emitting diodes (LED),[3,4] photovoltaics,[5–7] and imagers.[8] The size-dependent optical gap allows to tune the target wavelength in a wide range, from 825 to 1750 nm.[9–11] The fabrication of these devices typically requires the synthesis of PbS QDs,[12] followed by the evaporation of solvent to create a solid-state-film composed of closed-pack PbS QDs,[13] and finally the deposition of electrodes and charge transfer layers. The role of colloidal QDs film is not only for photoemission/photoabsorption but also for charge transport (charge injection/extraction). Therefore, the device performance relies on both optical and transport properties.[14–16]

It is well known that the optical gap and transport gap (electronic bandgap) differ by the electron-hole (e-h) binding energy, which is an important physical quantity for the e-h separation after photoabsorption. The e-h binding energy is not easily accessible experimentally since it requires the concomitant measurement of the electronic and optical gaps, and mainly optical gaps are reported in the literature.[9,17–20] Although analytic models of the e-h binding energy based on electrostatics have been developed,[21,22] qualitative validation using advanced computational methods remains necessary. It is also necessary to take into account

the effect of the environment such as the solvent for QDs in solution. Recent studies demonstrated possible solvation engineering[23,24] to optimize the device performance. In the final device, QDs are embedded in a dielectric environment, which could influence the electronic structure significantly and further affect the band-alignment with electrodes.[25–27]

In this work, we carried out a systematic study using various state-of-the-art *ab initio* methods, including many-body perturbation theory (MBPT), to explore the size and solvation effects on the electronic structure and the optical gap. Comparison between methodologies derived from Density Functional Theory (DFT) and MBPT, which is normally done for molecules[28–30] and atoms,[31,32] is made on QDs in this study. Besides, this work reveals a physical insight of the screening effect from the solvent and the QD itself due to neutral and charged excitation. Furthermore, a comparison on the e-h binding energies is made between different *ab initio* methods and an analytic model.

Structure of PbS QD Bulk PbS in rock salt structure is a semiconductor with a narrow but direct bandgap about 0.37-0.40 eV at room temperature.[33] Thanks to the quantum confinement effect, the bandgap of PbS QD is tunable with size. However, the stoichiometry of QD, namely the *Pb:S* ratio, may deviate from one, leading to a metallic QD (with Fermi level lies in conduction/valence band) or a QD with gap states,[34,35] in absence of surface passivation by ligands which contribute to remove the gap states by balancing the charge in QD.[36,37] It remains challenging to control the precise stoichiometry of QD.[38] Here, we consider PbS QD with clean surfaces in which the stoichiometry preservation is achieved by placing the origin of QD at the center of a cubic, formed by 12 PbS bonds, which can be visualized easily from the smallest PbS QD in Figure 1e. Therefore, the origin of QD is an inversion center to map a *Pb* atom to a *S* atom. We considered QDs terminated with (111) surfaces, which is expected for small PbS QD with a diameter less than 3 nm.[39] The atomic positions of QDs were relaxed using PBE functional. These QD structures in the absence of ligand should be regarded as model systems, which facilitates the study of the

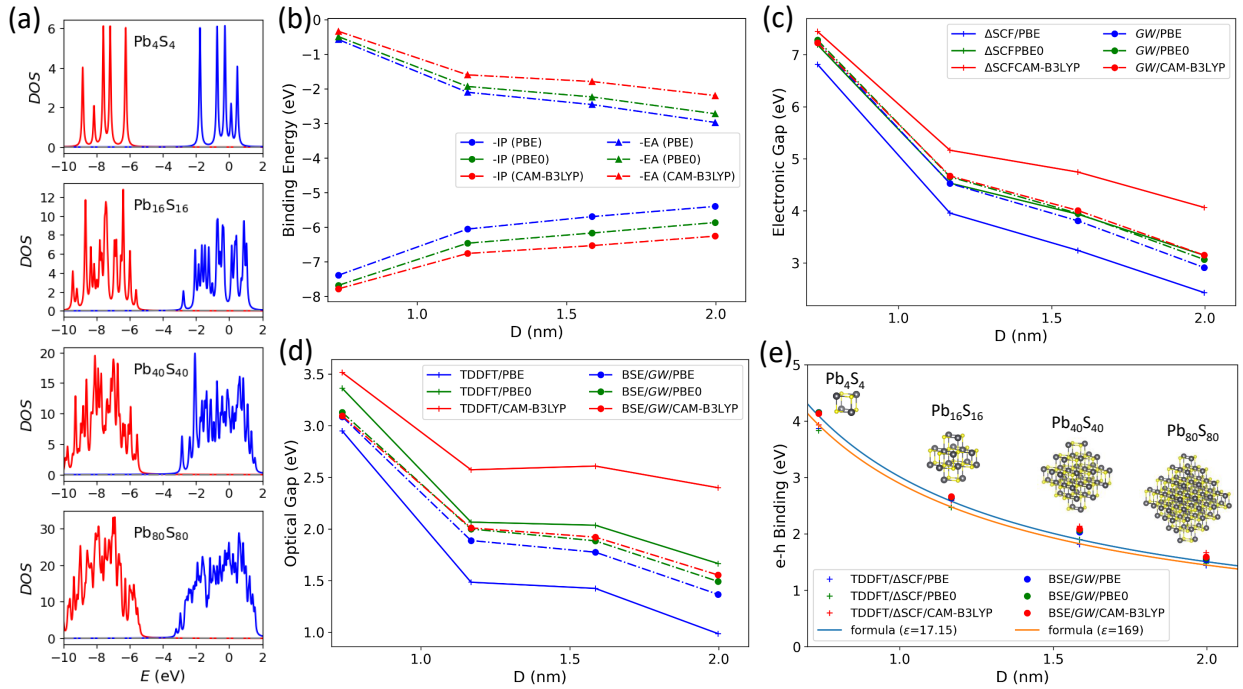

Figure 1: (a) Density of states obtained from DFT calculation for neutral QDs using PBE0 functional. Red/blue curve refer to HOMOs/LUMOs. No defect state appear in the band gap. (b) Ionization potential and electron affinity of QD as a function of its diameter. (c,d) Evolution of electronic and optical gap of QD with its diameter. (e) The e-h binding energy, which is the difference between electronic and optical gap, decreases rapidly with the increase of QD size. Inserts: Atomic structures of stoichiometry preserved PbS QDs.

Table 1: Summary of PbS quantum dots at various sizes computed using PBE functional. E_{HOMO}, E_{LUMO} and E_g^{DFT} are from DFT calculation for neutral QD. E_{IP} and E_{EA} are from ΔSCF method. The electronic gap $E_g = E_{IP} - E_{EA}$. S_1 is the first singlet exciton energy taking as the optical gap. The e-h binding energy ($E_{e,h}$) is difference between electronic and optical gaps. The electronic and optical gaps from eVGW/BSE starting from the DFT calculation using PBE are reported at the end. Energies are in eV.

	Pb_4S_4	$Pb_{16}S_{16}$	$Pb_{40}S_{40}$	$Pb_{80}S_{80}$
Diameter (nm)	0.74	1.17	1.59	2.00
DFT				
E_{HOMO}	-5.30	-4.77	-4.77	-4.66
E_{LUMO}	-2.38	-3.30	-3.35	-3.68
E_g^{DFT}	2.92	1.47	1.42	0.98
ΔSCF/TD-DFT				
E_{IP}	7.39	6.05	5.69	5.40
E_{EA}	0.57	2.10	2.45	2.97
E_g	6.81	3.96	3.24	2.43
S_1	2.95	1.48	1.42	0.99
$E_{e,h}$	3.87	2.47	1.82	1.44
GW/BSE				
E_g	7.24	4.53	3.81	2.91
S_1	3.09	1.89	1.77	1.37
$E_{e,h}$	4.15	2.64	2.03	1.54

size and solvent effect. Synthesizing these QDs might be challenging because of the active QD surfaces. Additionally, these QD structures contain both Pb- and S-terminated (111) surfaces. In contrast, experiments up to date suggests Pb-terminated (111) surfaces only.[40,41] Since these QDs are non-spherical, their effective diameter is defined as $D = (\frac{3Na^3}{4\pi})^{\frac{1}{3}}$, where N is the number of atoms, and $a = 5.9315$Å the lattice parameter of bulk PbS. The diameter varies from 0.7 to 2.0 nm.

Size effect Figure 1a presents the density of states of these QDs, obtained from DFT with PBE0 functional for neutral QD. Red and blue curves correspond to the HOMOs and LUMOs, respectively. Although the electronic structure depends on the choice of functional in DFT, we see the decrease of bandgap with the increase of QD size. In addition, there is no trap state lies in the bandgap, even though the surfaces of QDs are free of any passivation. This is expected for stoichiometric PbS QDs since, in contrast to III-V or II-VI

Table 2: Similar to Table 1, but for PBE0 functional.

	Pb_4S_4	$Pb_{16}S_{16}$	$Pb_{40}S_{40}$	$Pb_{80}S_{80}$
Diameter (nm)	0.74	1.17	1.59	2.00
DFT				
E_{HOMO}	-6.24	-5.61	-5.55	-5.40
E_{LUMO}	-1.76	-2.76	-2.84	-3.20
E_g^{DFT}	4.48	2.85	2.70	2.20
ΔSCF/TD-DFT				
E_{IP}	7.68	6.46	6.17	5.86
E_{EA}	0.49	1.93	2.23	2.72
E_g	7.19	4.53	3.94	3.15
S_1	3.36	2.07	2.04	1.67
$E_{e,h}$	3.83	2.47	1.90	1.48
GW/BSE				
E_g	7.28	4.65	3.95	3.06
S_1	3.13	2.00	1.88	1.49
$E_{e,h}$	4.15	2.65	2.06	1.57

semiconductors, there is no dangling bonds at the surface of rocksalt IV-VI compounds.[42]

To access IP and EA quantitatively, ΔSCF method was performed, namely we computed the difference of energies between two self-consistent DFT calculations in which we either remove or add an electron in the QD. Hence, IP/EA reads:

$$E_{IP} = E^+ - E^0;\ E_{EA} = E^0 - E^-, \tag{1}$$

where E^0, E^-, and E^+ are the ground state energies for neutral, anion (-1), and cation (+1) of QDs. Figure 1b shows the IP and EA obtained using PBE, PBE0, and CAM-B3LYP functional. With the increase of QD size, IP decreases and EA increases. The electronic gap, which is the difference between IP and EA, is reported in Figure 1c. We notice the discrepancy in the electronic gap can be more than 1 eV among the three functionals. Therefore, eVGW calculations were performed to serve as a reliable reference. The electronic gap from eVGW is almost the same no matter starting from PBE, PBE0 or CAM-B3LYP, and is similar to the electronic gap computed from PBE0 using ΔSCF method.

Figure 1d shows the optical gap of PbS QDs, which is taken from the first singlet excita-

Table 3: Similar to Table 1, but for CAM-B3LYP functional.

	Pb_4S_4	$Pb_{16}S_{16}$	$Pb_{40}S_{40}$	$Pb_{80}S_{80}$
Diameter (nm)	0.74	1.17	1.59	2.00
DFT				
E_{HOMO}	-7.23	-6.56	-6.45	-6.27
E_{LUMO}	-0.90	-1.87	-1.95	-2.31
E_g^{DFT}	6.33	4.69	4.50	3.96
ΔSCF/TD-DFT				
E_{IP}	7.78	6.76	6.53	6.26
E_{EA}	0.34	1.59	1.79	2.19
E_g	7.45	5.16	4.75	4.07
S_1	3.52	2.57	2.61	2.40
$E_{e,h}$	3.93	2.59	2.14	1.67
GW/BSE				
E_g	7.23	4.67	4.01	3.15
S_1	3.10	2.01	1.92	1.55
$E_{e,h}$	4.13	2.66	2.09	1.59

tion S_1. The functional dependency of TD-DFT results is obvious, but it is not the case for BSE, which is performed on top of eVGW calculation. Figure 1e shows the e-h binding energy, which is the difference between electronic and optical gaps. The functional dependency is less evident due to the cancellation of error, namely both electronic and optical gaps were over or under estimated. Remarkably, in spite of the functional dependency of the gaps, the size-dependent e-h binding energy is well described by the following analytic formula derived from electrostatic for spherical QD:[21]

$$E_{e,h} = 1.79\frac{e^2}{4\pi\epsilon_0\epsilon_{in}r} + \frac{e^2(\epsilon_{in}-\epsilon_{out})}{4\pi\epsilon_0\epsilon_{in}\epsilon_{out}r}, \tag{2}$$

where ϵ_{in} and ϵ_{out} are the dielectric constant of the QD and the environment, and r the radius of QD. Here the ϵ_{in} was set to 169 or 17.15 for the static dielectric constant with/without ionic contribution. The environmental dielectric constant is 1 for gas-phase.

The detail results for PBE, PBE0, and CAM-B3LYP functionals are tabulated in Tables 1,2, and 3.

Solvent effect

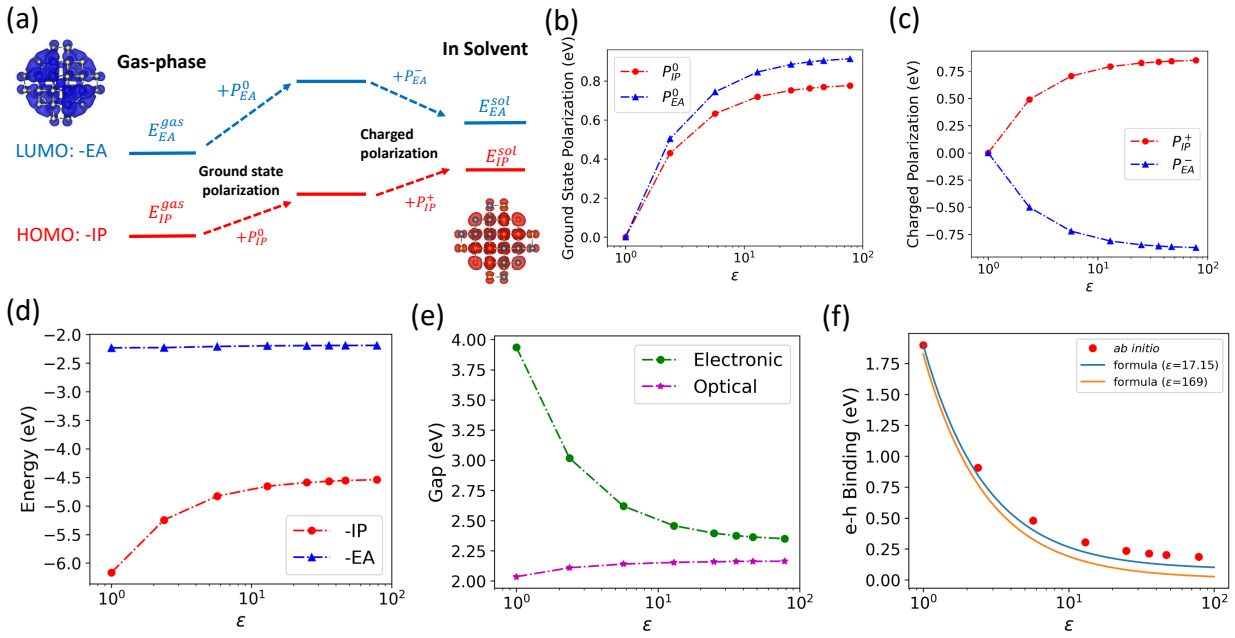

Figure 2: (a) Illustration of solvent effect on IP (HOMO) and EA (LUMO). The polarization effect from solvent can be decomposed into ground state polarization and charged polarization (see text for detail). Inserts: Averaged HOMO (red) and LUMO (blue) density of $Pb_{40}S_{40}$. (b,c) Ground state and charged polarization as a function of dielectric constant of solvent for a PbS QD of diameter 1.5 nm. (d) IP/EA and (e) the electronic/optical gaps versus dielectric constant of the PbS QD. Optical gap is stable while electronic gaps decreases rapidly results huge variation in e-h binding energy as shown by the red dots in (f). The solvent-dependent e-h binding energy is described by the analytical formula 2 (blue and red lines).

A solvent is polarized by the QDs due to 1) the multi-poles carried by QDs at ground state, even though they are neutral, and 2) the additional excitations (charged/neutral) in QDs. The former is so-called ground-state polarization, while the latter is charged polarization. Polarization charges bring an additional electric field acting on the electron states (wave function or molecular orbitals), resulting in the shift of molecular orbital energies. The shift due to the ground state polarization (P_i^0) is:

$$P_i^0 = E_i^{gas} - E_i^{sol}, \tag{3}$$

Table 4: Summary of the results obtained for $Pb_{40}S_{40}$ QDs in various solvents. ϵ is the dielectric constant of the solvent. E_{IP} and E_{EA} are from ΔSCF method in the presence of a solvent. E_g is the electronic gap. S_1 is the first singlet exciton energy taking as the optical gap. P^0_{IP} and P^0_{EA} are the shift of IP and EA due to ground state polarization. Similarly, P^+_{IP} and P^-_{EA} are due to charged excitation. The e-h binding energy ($E_{e,h}$) is the difference between electronic and optical gaps. Results are obtained using PBE0 functional. Energies are in eV.

	ε	E_{IP}	E_{EA}	E_g	S_1	P^0_{IP}	P^0_{EA}	P^+_{IP}	P^-_{EA}	$E_{e,h}$
Gas	1.000	6.167	2.232	3.935	2.036	0.000	0.000	0.000	0.000	1.899
Toluene	2.374	5.246	2.229	3.017	2.110	0.430	0.504	0.491	-0.501	0.907
Chlorobenzene	5.697	4.828	2.208	2.620	2.141	0.633	0.744	0.706	-0.720	0.479
Pyridine	12.978	4.655	2.197	2.458	2.154	0.719	0.846	0.793	-0.811	0.304
Ethanol	24.852	4.590	2.193	2.396	2.160	0.752	0.884	0.826	-0.846	0.236
Acetonitrile	35.688	4.568	2.192	2.376	2.162	0.763	0.897	0.837	-0.857	0.214
DMSO	46.826	4.556	2.191	2.365	2.163	0.769	0.904	0.843	-0.863	0.202
Water	78.355	4.540	2.190	2.350	2.164	0.776	0.914	0.851	-0.871	0.186

Table 5: Comparison of solvation effects for different mechanisms

Type	Interaction	Strength
Ground-state polarization	Multi-pole in neutral QD $\rightarrow$ solvent $\rightarrow$ Molecular orbital	Medium
Charged polarization	Additional charge in QD $\rightarrow$ solvent $\rightarrow$ Molecular orbital	Strong
Optical excitation	exciton in QD $\rightarrow$ solvent $\rightarrow$ exciton in QD	Weak

where E_i is the energy of ith molecular orbital obtained from DFT for neutral QD in gas-phase or solvent. The ground state polarization shifts all molecular orbital energies in the same direction, either up or down. The direction is governed by the sign of the multi-pole moment of the ground state. However, how much it shifts a particular level depends on the shape of the wave function. Taking a 1.5 nm diameter PbS QD ($Pb_{40}S_{40}$) with PBE0 functional as an example (Figure 2b), the shift on LUMO (EA) is more than HOMO (IP), suggesting LUMO has a delocalized wavefunction with larger weight on the outer shell of QD as shown in figure 2a. Therefore, the LUMO experiences a larger impact from the electric field due to the polarized charges in solvent.

ΔSCF allows the access of IP/EA of QDs in a solvent. Compared to the gas-phase, the shift on IP/EA sums effects from both ground state and charged polarizations, which is

illustrated by Figure 2a, as described in Ref.[26] Therefore, the IP/EA in a solvent is:

$$E_{IP}^{sol} = E_{IP}^{gas} + P_{IP}^{0} + P_{IP}^{+}; \tag{4}$$

$$E_{EA}^{sol} = E_{EA}^{gas} + P_{EA}^{0} + P_{EA}^{-}, \tag{5}$$

where $P^{\pm}$ is the shift due to the charged polarization. Figure 2c shows that the shift is in opposite direction for IP and EA, due to the opposite sign of charge (removes/adds an electron for IP/EA), resulting in a reduction of the electronic gap. The net shift on EA is small due to the sign difference between ground-state and charged polarization (opposite sign of P_{EA}^{0} and P_{EA}^{-}); however, it is constructive for IP.

Solvent has a much smaller impact on the optical gap, which increases slightly with the dielectric constant, similar to Ref.[43] This might originate from the interaction between polarized charge in solvent due to ground state dipole/multi-pole and the exciton, because the LUMO shifts slightly more than HOMO due to ground state polarization (Fig. 2b), as the first optical excitation involves heavily the HOMO to LUMO transition. Although optical excitation results in a multi-pole momentum from the generated e-h pair, which also polarizes the solvent, the electric field from the polarized charge could act on an exciton. However, this dipole $\rightarrow$ polarized charge $\rightarrow$ dipole interaction decays fast with distance resulting in only a small shift in exciton energy. Figure 2e shows the evolution of the electronic and optical gap versus the dielectric constant of solvents (values are reported in Table 4). The e-h binding energy is large in gas-phase (1.9 eV) and is dramatically reduced to less than 0.18 eV for QD in water. The solvation effect on e-h binding is also captured by the analytic formula (Eq. 2) by setting ϵ_{out} to the dielectric constant of the solvent.

Table 5 summarizes the different impacts of the screening effect from solvent due to different mechanisms: 1) multi-pole of neutral QD; 2) additional charge; 3) dipole by optical excitation.

Discussion and Conclusion Bulk PbS is known as a material with a large dielectric constant (static dielectric constant about 175, and optical dielectric constant about 16).[44,45] Previous work on PbS thin films shows that the dielectric constant does not change much with the thickness and remains at the bulk value.[46] By checking the size-dependent polarizability of QDs (see supporting information), it is linear with the volume of QD, implying a constant dielectric constant. Therefore, the fast decrease in e-h binding energy, from 4 eV to about 1.5 eV when the diameter is increased from 0.7 to 2.0 nm, should be interpreted as a volume effect, namely lack of polarizable medium. The presence of solvent further reduces the e-h binding energy by providing additional dielectric screening. Solvent with a large dielectric constant could limit the e-h binding energy to a small value, like 0.18 eV for a QD of 1.5 diameter in water.

The e-h binding energy obtained from *ab initio* methods, namely by using ΔSCF and TD-DFT for the electronic and optical gaps, is stable with the choice of functional. In additional, it is consistent with the many-body perturbation approach. Interestingly, the optical gap obtained using PBE functional is close to the HOMO-LUMO gap evaluated using a single DFT calculation for a neutral QD (see Table 1). This might be an efficient way to evaluate the e-h binding energy without performing TD-DFT calculation. Furthermore, both the size and the solvent effect on the e-h binding energy is well described by the analytic formula.

Solvent screens both charges and dipoles in QD, resulting in a shift of the energies for molecular orbitals and excitons. The electronic structure of QD is influenced by both the ground state polarization and charged polarization by solvent. Such a shift in electronic structure would affect the band alignment with electrodes, which influences the carrier injection/extraction. In contrast, the solvent has a limited impact on optical excitation.

Methods

Density functional theory (DFT) with Gaussian basis (def2-SVP)[47] is employed to access the ground state energy and energy levels of molecular orbitals. Three types of functional were used: 1) a semi-local density functional (PBE),[48] 2) an hybrid functional (PBE0),[49] and 3) a range-separated hybrid functional (CAM-B3LYP).[50] The ionization potential (IP) and electron affinity (EA) are evaluated using the ΔSCF method, which is more stable with the choice of functional compared to energies of HOMO (Highest Occupied Molecular Orbital) and LUMO (Lowest Unoccupied Molecular Orbital) from a single DFT calculation for neutral QD.[51] The optical excitation is calculated using time-dependent density functional theory (TD-DFT) beyond the Tamm-Damcoff approximation on top of DFT calculation for neutral QD. The solvent is described using the SMD continuum solvation model[52] in both DFT and TD-DFT. All DFT and TD-DFT were performed using *ORCA* quantum chemistry code.[53] Electronic gap and optical excitation were also computed using many-body perturbation theory, i.e. eigenvalue corrected *GW* calculation (eV*GW*) and Bethe-Salpeter Equations (BSE), using *Fiesta* package[54] with DFT starting point from *NWChem* quantum chemistry code[55] using the same basis set. The convergence of the Gaussian basis for DFT, TD-DFT, *GW* and BSE calculations are reported in the supplemental material. Test calculation including spin-orbit coupling and relativistic effect (ZORA) for the Pb_4S_4 QD does not show any significant impact on the results obtained from a non-relativistic calculation in the absence of spin-orbit coupling.

Acknowledgement

B. S. and J. L. thank the allocation of computational resource from GENCI–IDRIS (Grant 2020-A0090912036 and Grant 2021-A0110912036). We acknowledge X. Blase and I. Duchemin as the inventor and major contributors of *Fiesta* package, the code used for *GW* and BSE calculations in this work.

Supporting Information Available

Convergence of basis set and size-dependent polarizability of PbS QD are available in supplement information.

References

(1) Eisler, H.-J.; Sundar, V. C.; Bawendi, M. G.; Walsh, M.; Smith, H. I.; Klimov, V. Color-Selective Semiconductor Nanocrystal Laser. *Applied Physics Letters* **2002**, *80*, 4614–4616.

(2) Whitworth, G. L.; Dalmases, M.; Taghipour, N.; Konstantatos, G. Solution-Processed PbS Quantum Dot Infrared Laser with Room-Temperature Tunable Emission in the Optical Telecommunications Window. *Nature Photonics* **2021**, *15*, 738–742.

(3) Rogach, A. L.; Gaponik, N.; Lupton, J. M.; Bertoni, C.; Gallardo, D. E.; Dunn, S.; Li Pira, N.; Paderi, M.; Repetto, P.; Romanov, S. G.; O'Dwyer, C.; Sotomayor Torres, C. M.; Eychmüller, A. Light-Emitting Diodes with Semiconductor Nanocrystals. *Angewandte Chemie International Edition* **2008**, *47*, 6538–6549.

(4) Zhang, X.; Chen, Y.; Lian, L.; Zhang, Z.; Liu, Y.; Song, L.; Geng, C.; Zhang, J.; Xu, S. Stability Enhancement of PbS Quantum Dots by Site-Selective Surface Passivation for Near-Infrared LED Application. *Nano Research* **2021**, *14*, 628–634.

(5) Ganesan, A. A.; Houtepen, A. J.; Crisp, R. W. Quantum Dot Solar Cells: Small Beginnings Have Large Impacts. *Applied Sciences* **2018**, *8*, 1867.

(6) Choi, M.-J.; García De Arquer, F. P.; Proppe, A. H.; Seifitokaldani, A.; Choi, J.; Kim, J.; Baek, S.-W.; Liu, M.; Sun, B.; Biondi, M.; et Al., Cascade Surface Modification of Colloidal Quantum Dot Inks Enables Efficient Bulk Homojunction Photovoltaics. *Nature Communications* **2020**, *11*, 103.

(7) Sukharevska, N.; Bederak, D.; Goossens, V. M.; Momand, J.; Duim, H.; Dirin, D. N.; Kovalenko, M. V.; Kooi, B. J.; Loi, M. A. Scalable PbS Quantum Dot Solar Cell Production by Blade Coating from Stable Inks. *ACS Applied Materials and Interfaces* **2021**, *13*, 5195–5207.

(8) Choi, H. T.; Kang, J.-H.; Ahn, J.; Jin, J.; Kim, J.; Park, S.; Kim, Y.-H.; Kim, H.; Song, J. D.; Hwang, G. W.; Im, S.; Shim, W.; Lee, Y. T.; Park, M.-C.; Hwang, D. K. Zero-Dimensional PbS Quantum Dot–InGaZnO Film Heterostructure for Short-Wave Infrared Flat-Panel Imager. *ACS Photonics* **2020**, *7*, 1932–1941.

(9) Moreels, I.; Lambert, K.; Smeets, D.; De Muynck, D.; Nollet, T.; Martins, J. C.; Vanhaecke, F.; Vantomme, A.; Delerue, C.; Allan, G.; et Al., Size-Dependent Optical Properties of Colloidal PbS Quantum Dots. *ACS Nano* **2009**, *3*, 3023–3030.

(10) Moreels, I.; Justo, Y.; De Geyter, B.; Haustraete, K.; Martins, J. C.; Hens, Z. Size-Tunable, Bright, and Stable PbS Quantum Dots: A Surface Chemistry Study. *ACS Nano* **2011**, *5*, 2004–2012.

(11) Christodoulou, S.; Ramiro, I.; Othonos, A.; Figueroba, A.; Dalmases, M.; Özdemir, O.; Pradhan, S.; Itskos, G.; Konstantatos, G. Single-Exciton Gain and Stimulated Emission Across the Infrared Telecom Band from Robust Heavily Doped PbS Colloidal Quantum Dots. *Nano Letters* **2020**, *20*, 5909–5915.

(12) Reiss, P.; Carrière, M.; Lincheneau, C.; Vaure, L.; Tamang, S. Synthesis of Semiconductor Nanocrystals, Focusing on Nontoxic and Earth-Abundant Materials. *Chemical Reviews* **2016**, *116*, 10731–10819.

(13) Pejović, V.; Lee, J.; Georgitzikis, E.; Li, Y.; Kim, J. H.; Lieberman, I.; Malinowski, P. E.; Heremans, P.; Cheyns, D. Thin-Film Photodetector Optimization for High-Performance Short-Wavelength Infrared Imaging. *IEEE Electron Device Letters* **2021**, *42*, 1196–1199.

(14) Yazdani, N.; Andermatt, S.; Yarema, M.; Farto, V.; Bani-Hashemian, M. H.; Volk, S.; Lin, W. M. M.; Yarema, O.; Luisier, M.; Wood, V. Charge Transport in Semiconductors Assembled from Nanocrystal Quantum Dots. *Nature Communications* **2020**, *11*, 2852.

(15) Biondi, M.; Choi, M.-J.; Wang, Z.; Wei, M.; Lee, S.; Choubisa, H.; Sagar, L. K.; Sun, B.; Baek, S.-W.; Chen, B.; et Al., Facet-Oriented Coupling Enables Fast and Sensitive Colloidal Quantum Dot Photodetectors. *Advanced Materials* **2021**, *33*, 2101056.

(16) Hartley, C. L.; Kessler, M. L.; Dempsey, J. L. Molecular-Level Insight into Semiconductor Nanocrystal Surfaces. *Journal of the American Chemical Society* **2021**, *143*, 1251–1266.

(17) Cademartiri, L.; Montanari, E.; Calestani, G.; Migliori, A.; Guagliardi, A.; Ozin, G. A. Size-Dependent Extinction Coefficients of PbS Quantum Dots. *Journal of the American Chemical Society* **2006**, *128*, 10337–10346.

(18) Brown, P. R.; Kim, D.; Lunt, R. R.; Zhao, N.; Bawendi, M. G.; Grossman, J. C.; Bulović, V. Energy Level Modification in Lead Sulfide Quantum Dot Thin Films Through Ligand Exchange. *ACS Nano* **2014**, *8*, 5863–5872.

(19) Weidman, M. C.; Beck, M. E.; Hoffman, R. S.; Prins, F.; Tisdale, W. A. Monodisperse, Air-Stable PbS Nanocrystals Via Precursor Stoichiometry Control. *ACS Nano* **2014**, *8*, 6363–6371.

(20) Poddubny, A. N.; Litvyak, V. M.; Nestoklon, M. O.; Cherbunin, R. V.; Golubkov, V. V.; Onushchenko, P. A.; Babkina, A. N.; Onushchenko, A. A.; Goupalov, S. V. Role of Valley Anisotropy in Optical Absorption of Monodisperse PbS Nanocrystals. *The Journal of Physical Chemistry C* **2017**, *121*, 27766–27773.

(21) Delerue, C.; Lannoo, M. *Nanostructures: Theory and Modeling*; 2004.

(22) Brus, L. E. Electron–electron and Electron-hole Interactions in Small Semiconductor Crystallites: The Size Dependence of the Lowest Excited Electronic State. *The Journal of Chemical Physics* **1984**, *80*, 4403–4409.

(23) Mathew, K.; Sundararaman, R.; Letchworth-Weaver, K.; Arias, T. A.; Hennig, R. G. Implicit Solvation Model for Density-Functional Study of Nanocrystal Surfaces and Reaction Pathways. *The Journal of Chemical Physics* **2014**, *140*, 084106.

(24) Wu, R.; Yang, Y.; Li, M.; Qin, D.; Zhang, Y.; Hou, L. Solvent Engineering for High-Performance PbS Quantum Dots Solar Cells. *Nanomaterials* **2017**, *7*.

(25) Li, J.; D'Avino, G.; Duchemin, I.; Beljonne, D.; Blase, X. Combining the Many-Body GW Formalism with Classical Polarizable Models: Insights on the Electronic Structure of Molecular Solids. *The Journal of Physical Chemistry Letters* **2016**, *7*, 2814–2820.

(26) Li, J.; D'Avino, G.; Duchemin, I.; Beljonne, D.; Blase, X. Accurate Description of Charged Excitations in Molecular Solids from Embedded Many-Body Perturbation Theory. *Physical Review B* **2018**, *97*, 035108.

(27) Li, J.; Duchemin, I.; Roscioni, O. M.; Friederich, P.; Anderson, M.; Da Como, E.; Kociok-Köhn, G.; Wenzel, W.; Zannoni, C.; Beljonne, D.; Blase, X.; D'Avino, G. Host Dependence of the Electron Affinity of Molecular Dopants. *Materials Horizons* **2019**, *6*, 107–114.

(28) Li, J.; Olevano, V. Hydrogen-Molecule Spectrum by the Many-Body *GW* Approximation and the Bethe-Salpeter Equation. *Physical Review A* **2021**, *103*, 012809.

(29) Van Setten, M. J.; Caruso, F.; Sharifzadeh, S.; Ren, X.; Scheffler, M.; Liu, F.; Lischner, J.; Lin, L.; Deslippe, J. R.; Louie, S. G.; Yang, C.; Weigend, F.; Neaton, J. B.; Evers, F.; Rinke, P. GW100: Benchmarking G0W0 for Molecular Systems. *Journal of Chemical Theory and Computation* **2015**, *11*, 5665–5687.

(30) Jacquemin, D.; Duchemin, I.; Blase, X. 0–0 Energies Using Hybrid Schemes: Benchmarks of TD-DFT, CIS(D), ADC(2), CC2, and BSE/GW Formalisms for 80 Real-Life Compounds. *Journal of Chemical Theory and Computation* **2015**, *11*, 5340–5359.

(31) Li, J.; Holzmann, M.; Duchemin, I.; Blase, X.; Olevano, V. Helium Atom Excitations by the G W and Bethe-Salpeter Many-Body Formalism. *Physical Review Letters* **2017**, *118*, 163001.

(32) Li, J.; Drummond, N. D.; Schuck, P.; Olevano, V. Comparing Many-Body Approaches Against the Helium Atom Exact Solution. *SciPost Physics* **2019**, *6*, 040.

(33) Svane, A.; Christensen, N. E.; Cardona, M.; Chantis, A. N.; Van Schilfgaarde, M.; Kotani, T. Quasiparticle Self-Consistent GW Calculations for PbS, PbSe, and PbTe: Band Structure and Pressure Coefficients. *Physical Review B* **2010**, *81*, 245120.

(34) Kim, D.; Kim, D.-H.; Lee, J.-H.; Grossman, J. C. Impact of Stoichiometry on the Electronic Structure of PbS Quantum Dots. *Physical Review Letters* **2013**, *110*, 196802.

(35) Giansante, C.; Infante, I. Surface Traps in Colloidal Quantum Dots: A Combined Experimental and Theoretical Perspective. *The Journal of Physical Chemistry Letters* **2017**, *8*, 5209–5215.

(36) Ip, A. H. et al. Hybrid Passivated Colloidal Quantum Dot Solids. *Nature Nanotechnology* **2012**, *7*, 577–582.

(37) Ghosh, S.; Manna, L. The Many "Facets" of Halide Ions in the Chemistry of Colloidal Inorganic Nanocrystals. *Chemical Reviews* **2018**, *118*, 7804–7864.

(38) Balazs, D. M.; Bijlsma, K. I.; Fang, H.-H.; Dirin, D. N.; Döbeli, M.; Kovalenko, M. V.; Loi, M. A. Stoichiometric Control of the Density of States in PbS Colloidal Quantum Dot Solids. *Science Advances* **2017**, *3*, eaao1558.

(39) Beygi, H.; Sajjadi, S. A.; Babakhani, A.; Young, J. F.; Van Veggel, F. C. J. M. Surface Chemistry of As-Synthesized and Air-Oxidized PbS Quantum Dots. *Applied Surface Science* **2018**, *457*, 1–10.

(40) Choi, H.; Ko, J.-H.; Kim, Y.-H.; Jeong, S. Steric-Hindrance-Driven Shape Transition in PbS Quantum Dots: Understanding Size-Dependent Stability. *Journal of the American Chemical Society* **2013**, *135*, 5278–5281.

(41) Zherebetskyy, D.; Scheele, M.; Zhang, Y.; Bronstein, N.; Thompson, C.; Britt, D.; Salmeron, M.; Alivisatos, P.; Wang, L.-W. Hydroxylation of the Surface of PbS Nanocrystals Passivated with Oleic Acid. *Science* **2014**, *344*, 1380–1384.

(42) Allan, G.; Delerue, C. Confinement Effects in PbSe Quantum Wells and Nanocrystals. *Physical Review B* **2004**, *70*, 245321.

(43) Garoufalis, C. S.; Zeng, Z.; Bester, G.; Galanakis, I.; Hayrapetyan, D.; Paspalakis, E.; Baskoutas, S. Excitons in ZnO Quantum Dots: The Role of Dielectric Confinement. *The Journal of Physical Chemistry C* **2022**, *126*, 2833–2838.

(44) Zemel, J. N.; Jensen, J. D.; Schoolar, R. B. Electrical and Optical Properties of Epitaxial Films of PbS, PbSe, PbTe, and SnTe. *Physical Review* **1965**, *140*, A330–A342.

(45) Dalven, R. In *Solid State Physics*; Ehrenreich, H., Seitz, F., Turnbull, D., Eds.; Academic Press, 1974; Vol. 28; p 179–224.

(46) Moreels, I.; Allan, G.; De Geyter, B.; Wirtz, L.; Delerue, C.; Hens, Z. Dielectric Function of Colloidal Lead Chalcogenide Quantum Dots Obtained by a Kramers-Krönig Analysis of the Absorbance Spectrum. *Physical Review B* **2010**, *81*, 235319.

(47) Weigend, F.; Ahlrichs, R. Balanced Basis Sets of Split Valence, Triple Zeta Valence and Quadruple Zeta Valence Quality for H to Rn: Design and Assessment of Accuracy. *Physical Chemistry Chemical Physics* **2005**, *7*, 3297–3305.

(48) Perdew, J. P.; Burke, K.; Ernzerhof, M. Generalized Gradient Approximation Made Simple. *Physical Review Letters* **1996**, *77*, 3865–3868.

(49) Perdew, J. P.; Ernzerhof, M.; Burke, K. Rationale for Mixing Exact Exchange with Density Functional Approximations. *The Journal of Chemical Physics* **1996**, *105*, 9982–9985.

(50) Yanai, T.; Tew, D. P.; Handy, N. C. A New Hybrid Exchange–correlation Functional Using the Coulomb-Attenuating Method (CAM-B3LYP). *Chemical Physics Letters* **2004**, *393*, 51–57.

(51) Dittmer, A.; Izsák, R.; Neese, F.; Maganas, D. Accurate Band Gap Predictions of Semiconductors in the Framework of the Similarity Transformed Equation of Motion Coupled Cluster Theory. *Inorganic Chemistry* **2019**, *58*, 9303–9315.

(52) Marenich, A. V.; Cramer, C. J.; Truhlar, D. G. Universal Solvation Model Based on Solute Electron Density and on a Continuum Model of the Solvent Defined by the Bulk Dielectric Constant and Atomic Surface Tensions. *The Journal of Physical Chemistry B* **2009**, *113*, 6378–6396.

(53) Neese, F. Software Update: The ORCa Program System, Version 4.0. *WIREs Computational Molecular Science* **2018**, *8*, E1327.

(54) Blase, X.; Attaccalite, C.; Olevano, V. First-Principles GW Calculations for Fullerenes, Porphyrins, Phtalocyanine, and Other Molecules of Interest for Organic Photovoltaic Applications. *Physical Review B* **2011**, *83*, 115103.

(55) Valiev, M.; Bylaska, E. J.; Govind, N.; Kowalski, K.; Straatsma, T. P.; Van Dam, H. J. J.; Wang, D.; Nieplocha, J.; Apra, E.; Windus, T. L.; De Jong, W. A. NWChem: A Comprehensive and Scalable Open-Source Solution for Large Scale Molecular Simulations. *Computer Physics Communications* **2010**, *181*, 1477–1489.

Supporting Information: Size and Solvation Effects on Electronic and Optical Properties of PbS Quantum Dots

Benoît Sklénard,[†] Gabriel Mugny,[‡] Bilal Chehaibou,[¶] Christophe Delerue,[¶] Arthur Arnaud,[§] and Jing Li[*,†]

†*Univ. Grenoble Alpes, CEA, Leti, F-38000, Grenoble, France*

‡*STMicroelectronics, 12 rue Jules Horowitz, 38019 Grenoble, France*

¶*Univ. Lille, CNRS, Centrale Lille, Univ. Polytechnique Hauts-de-France, Junia, UMR 8520—IEMN, F-59000 Lille, France*

§*STMicroelectronics, 850 rue J. Monnet, 38926 Crolles, France*

E-mail: Jing.Li@cea.fr

Convergence test for basis set

The convergence of the basis set has been tested among double, triple, and quadruple basis sets (def2-SVP, def2-TZVP, and def2-QZVP) for Pb_4S_4 QD using PBE0 functional. Table 1 shows that the electronic gap from ΔSCF is converged within 0.2 eV, and the optical gap from TD-DFT is converged within 0.1 eV using def2-SVP basis. Meanwhile, the electronic gap from *GW* is converged within 0.1 eV, and the optical gap from BSE is converged within 0.15 eV using def2-SVP basis.

Table 1: Convergence test for Pb_4S_4 QD using PBE0 functional but different basis-sets. E_{HOMO}, E_{LUMO} and E_g^{DFT} are from DFT calculation for neutral QD. E_{IP} and E_{EA} are from ΔSCF method. The electronic gap $E_g = E_{IP} - E_{EA}$. S_1 is the first singlet exciton energy taking as the optical gap. The e-h binding energy ($E_{e,h}$) is difference between electronic and optical gaps. The electronic and optical gaps from e$V GW$/BSE starting from the DFT calculation using PBE0 are reported at the end. Energies are in eV.

	def2-SVP	def2-TZVP	def2-QZVP
DFT			
E_{HOMO}	-6.237	-6.273	-6.278
E_{LUMO}	-1.761	-1.834	-1.851
E_g^{DFT}	4.476	4.440	4.427
ΔSCF/TD-DFT			
E_{IP}	7.680	7.657	7.649
E_{EA}	0.489	0.632	0.678
E_g	7.190	7.025	6.971
S_1	3.362	3.332	3.321
$E_{e,h}$	3.828	3.693	3.650
GW/BSE			
E_g	7.281	7.131	7.284
S_1	3.129	3.114	3.265
$E_{e,h}$	4.152	4.017	4.019

Size dependence of polarizability in PbS QD

By applying a constant electric field along the x direction, we examed the induced dipole (along the x direction) of PbS QD at different sizes. The figure below shows that the induced dipole is proportional to the volume of the QD (see figure below). Therefore, the reduction of the screening effect with the decrease in QD size is a volumic effect, namely lack of polarizable medium, but not the change of dielectric constant.

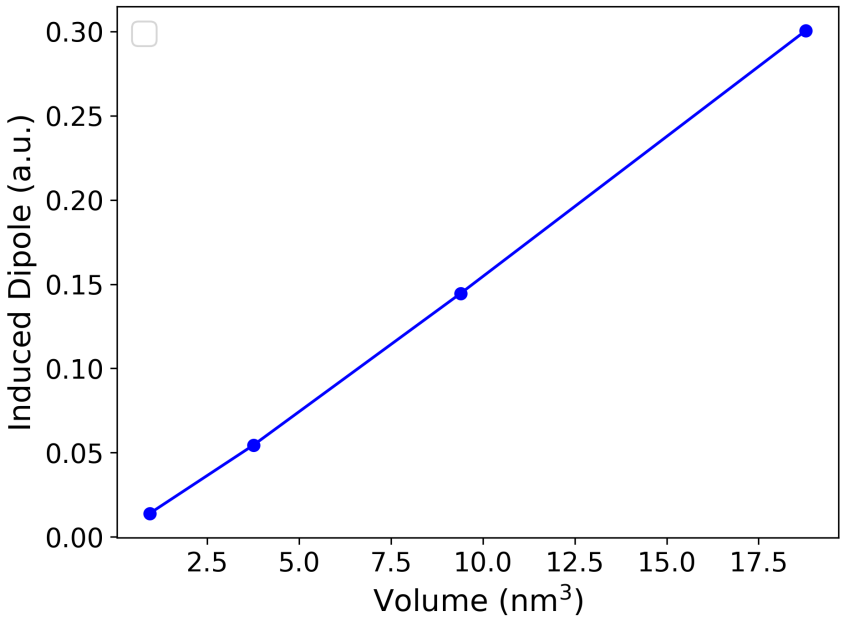

Figure 1: Induced dipole in PbS QD at various size versus volume of QD with external electric field (0.1 mV/Å)